RSC Advances

ROYAL SOCIETY OF CHEMISTRY

www.rsc.org/advances

Graphical Abstract

Novel RGO/AgNDs composite was prepared by one-step electrodeposition method. The RGO/AgNDs composite performed excellent photoelectrical conversion and sensitive electrochemical response to H_2O_2.

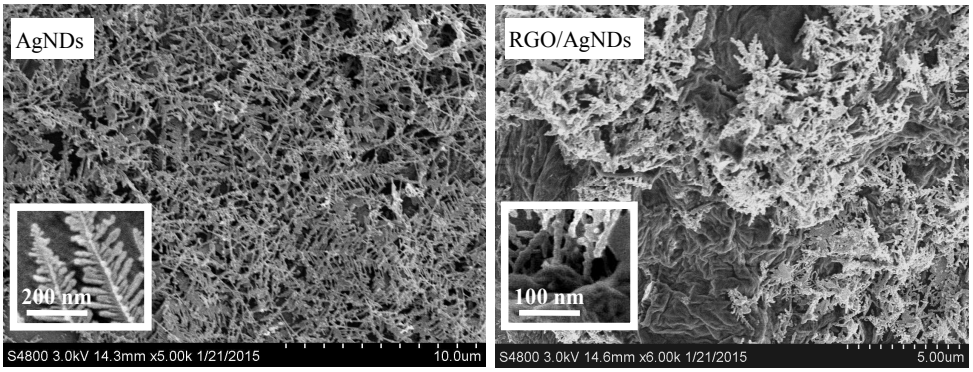

Electrochemical Synthesis and Photoelectrochemical Property of Novel RGO/AgNDs Composite

Xiaomei Zhang, Aming Wang, Rui Ke, Shengyi Zhang*, Helin Niu, Changjie Mao, Jiming Song, Baokang Jin, Yupeng Tian

Department of Chemistry, Anhui University, Hefei 230601, China

*Corresponding author. E-mail: syzhangi@126.com

Abstract:

A novel composite of Ag nanodendrites (AgNDs) wrapped with reduced graphene oxide (RGO) was prepared via one-step electrodeposition approach. The characterization results show that three dimensional (3D) AgNDs with cubic phase are enwrapped by RGO sheets in the RGO/AgNDs composite as-prepared. Due to the synergistic effect of AgNDs and RGO, the RGO/AgNDs composite performed excellent photoelectrical conversion. Furthermore, depend on its good electrochemical response to H_2O_2, the electrode modified with RGO/AgNDs composite was used as a sensor for H_2O_2 detection, and the results show that the detection linear range is from 0.08 mM to 2.65 mM.

Keywords: Silver nanodendrites; Graphene; Composite; Photoelectric conversion; Electrochemical sensor

1. Introduction

In the past decades, the considerable effort of researchers has been devoted to develop new energy conversion and storage devices, due to ever-increasing environmental problems and up-coming fossil-fuel depletion. Among diverse devices,

the solar cells that harvest solar energy by photoelectric conversion have received considerable attention. In solar cells, as well-known, the electrode material is the determinant of photoelectric conversion efficiency. Therefore, a variety of electrode materials, such as crystal silicon, chalcogenide, metal nanomaterial, carbon material and organic/inorganic hybrid, have been explored.[1-4] Graphene, an intriguing novel two-dimensional carbon material, has become a research hotspot since discovered in 2004, because of its unique structure and excellent properties.[5-8] By virtue of its good optical transmittance and electrical conductivity, graphene has been used as the electrode material of solar cells.[9-12] In other side, the large specific surface area of graphene makes it a good candidate for nano-scale substrate in fabrication of flexible composite materials. For example, by combining Au nanoparticles with graphene, Wang and co-workers fabricated an electrochemical detection platform.[13] Chakrabarti and co-workers reviewed the progress in the electrochemical modification of graphene-based materials,[14] and Chowdhury and co-worker summarized the photocatalytic property and application of graphene/semiconductor nanocomposites.[15]

As well-known, Ag materials with nanostructure have been widely studied because of their photophysical and photochemical properties. For example, based on their surface plasmon resonance (SPR) effect and strong absorption in the visible light region, Ag nanoparticles have been proposed as visible-light-activated photocatalysts. Recently, the Ag nanoparticles were composited with graphene, and the composites as-formed were used in surface enhanced Raman (SER) substrates, sensors and catalysts.[16-22] As a kind of dendritic materials with hierarchical structures and high aspect ratio, Ag nanodendrites (AgNDs) attracted much attention, due to their excellent performance in electron transport, surface enhanced Raman spectroscopy (SERS) and catalytic sensors.[23-25] In this work, the AgNDs were combined with

reduced graphene oxide (RGO) by in situ electrodeposition. Significantly, the RGO/AgNDs composite as-formed displayed an excellent photoelectric conversion. In addition, depend on the unique catalytic property of AgNDs,[26-27] the RGO/AgNDs composite was used as electrochemical sensor for H_2O_2 detection.

2. Experimental section

2.1. Materials and Instruments

Graphite powder (99.995%) and potassium permanganate ($KMnO_4$) were purchased from Shanghai Chemical Reagent Co. Ltd. Silver nitrate was obtained from Sinopharm Chemical Reagent Co., Ltd. Potassium iodide and Sodium sulfide were bought from Brady Bengbu Chemical Research Institute and Shanghai Tongya Chemical Technology Development Co., Ltd, respectively. Hydrogen peroxide 30% was obtained from Sinopharm Chemical Reagent Co.,Ltd. All reagents were of analytical grade and used as obtained. The solutions were all prepared with ultrapure water.

Electrochemical work station (CHI660E, Shanghai Chenhua Instruments Ltd, China); X-ray diffractometer (XRD, Rigaku D/max-RA, graphite monochromatized Cukα1 radiation, λ-0.15406 nm); Scanning electron microscope (SEM, S4800, Hitachi); Transmission electron microscopy (TEM, JEM-2100, JEOL, Japan); Xenon lamp (PLS-SXE300/300UV, Beijing Park Philae Science and Technology Co., Ltd).

2.2. Preparation of RGO/AgNDs composite

In advance, graphene oxide (GO) was prepared by a modified Hummers method,[28] and the GO solution (1mg/mL) was prepared by dispersing 20 mg GO in 20 mL water under sonicated. Typically, RGO/AgNDs composite was prepared by electrodeposition as follows. First, a piece of the indium tin oxide glass (ITO, 4 cm^2) was washed with acetone and ethanol respectively, and dried with nitrogen blow. The

three-electrode system was set up by cleaned ITO slice (WE), platinum wire (CE) and Ag/AgCl electrode (RE) against which all potentials were recorded. Then, the electrolyte solution was prepared by adding 400 μL 1mg/mL solution of GO into 15 mL mixture solution containing 0.01 M $AgNO_3$ and 0.1 M KNO_3. Finally, with three-electrode system, the RGO/AgNDs composite was produced on ITO slice by electrodepositing at -1.2 V for 200 s in electrolyte solution that had been bubbled with N_2 for 10 min beforehand. By similar electrodeposition as above, the RGO was prepared in absence of $AgNO_3$, and the AgNDs was prepared in absence of GO, respectively. Before electrodeposition, the cycle voltammograms of GO, $AgNO_3$ and GO/$AgNO_3$ solutions had been measured respectively, for exploring their electrode reactions.

2.3 Characterization and measurements

The products as-prepared were characterized by XRD, UV, SEM and EIS, respectively. Using the ITO slice covered with electrodeposition product as work electrode and a Xe lamp (100 mW/cm^2) as light source, typically, the measurements for photoelectric conversion were carried out in 0.1 M Na_2S solution. Using the ITO slice covered with RGO/AgNDs composite as sensor, the measurements for electrochemical response to H_2O_2 were performed in 1 M H_2SO_4 solution that had been deaerated. The Nyquist plots of electrochemical impedance spectroscopy (EIS) were measured in 0.01 M PBS (pH=7.4) solution containing 0.002 M $Fe(CN)_6^{4-/3-}$ and 0.1 M KCl, using same three-electrode system as above except that the Ag/AgCl electrode was replaced by saturated calomel electrode (SCE).

3. Results and discussion

3.1 Characterization

Fig.1A shows the cycle voltammograms of GO, $AgNO_3$ and GO/$AgNO_3$ solutions.

As shown on CV curve of $AgNO_3$ solution, the cathodic current at 0~-0.3 V belongs to the reduction of silver ions to silver atoms ($Ag^+ + e^- \rightarrow Ag$), and then the rising cathodic current produced over -0.4 V resulted from the reduction of dissolved oxygen by the catalysis of fresh Ag particles. Obviously, on the CV curve of the GO solution, there are a cathodic peak (at -1.30 V) and an anodic peak (at -0.85 V). According to the results reported,[19,29] the cathodic peak came from the reduction of active oxygen-containing groups on graphene sheets, and the anodic peak resulted from the oxidation of conjugated bonds on graphene sheets. For mixture solution containing GO and $AgNO_3$, there are two cathodic peaks (at -0.81 V and -1.17 V, respectively) on the CV curve, which is explained as follows. In aqueous solution, the hydroxyl and carboxyl groups on the GO sheets could dissociate to negatively charged species (GO^-) that combined with Ag^+ to form GO^-Ag^+ complex. Therefore, the reduction peak of the GO positively shifted from -1.30 V to -1.17 V, and the reduction peak of free Ag^+ ions negatively shifted from about -0.2 V to -0.81 V, due to the formation of GO^-Ag^+ complex. Furthermore, the oxidation peak (at -0.85 V) of pure GO disappeared on the CV curve of mixture solution, which suggests that the formation of the GO^-Ag^+ complex restrained the re-oxidation of reduced GO. Noteworthily, the reduction current of the mixture solution is much larger than that of pure GO or $AgNO_3$ solution, which may result from that the formation of GO^-Ag^+ complex promoted the electrode reactions.

Based on the results obtained as above, the electroreduction potential for mixture solution of GO and $AgNO_3$ was set at -1.20 V where the RGO and AgNDs could be synchronously electrodeposited on the surface of the ITO. The experiment results show that when the electroreduction potential was negatively shifted (such as, to -1.4 V), the electrodeposition productivity declined and the RGO/AgNDs composite

as-formed could not adhere on ITO firmly, since other species (such as H^+) in electrolyte solution were reduced, which interfered the formation of the composite.

Fig.1 (A) The cycle voltammograms obtained in different solutions (at scan rate of 25 mVs^{-1}); (B) XRD patterns of the products; (C) SEM image of pure Ag product (insert: enlarged part image); (D) SEM image of RGO/AgNDs composite (insert: enlarged part image of TEM).

Fig.1B shows the XRD patterns of the products electrodeposited with different electrolyte solutions. On the XRD pattern of the GO, there is a feature diffraction peak (at about 11°) of GO. For the product electrodeposited with GO, however, the diffraction peak of the GO disappeared, and there is a weak wide diffraction peak (at about 26°) on the XRD pattern of the product, which suggests the formation of RGO.[29] For the Ag product, the diffraction peaks on the XRD pattern can be indexed to the cubic phase of Ag (JCPDS Card, 00-001-1167).[30-31] Noticeably, on the XRD pattern of RGO/AgNDs composite, all of the sharp diffraction peaks agree well with that of the AgNDs, and the wide diffraction peak of RGO is very weak since the AgNDs were embedded into RGO sheets. According to the result reported in literature,[19] the diffraction peaks marked as "Δ" resulted from the ITO itself. The SEM image of pure Ag product is shown in Fig. 1C. Clearly, the product is made up of large-area dispersed 3D dendritic structures. From insert in Fig. 1C, it is observed that the long trunks as well as their branches are composed of many nanoparticles. As described in the literature,[32-33] the dendritic structure was formed according to diffusion-limited aggregation (DLA) mechanism. The SEM image (Fig. 1D) of RGO/AgNDs composite reveals the synthetic structure of RGO and AgNDs. Since the AgNDs and RGO were synchronously produced, the Ag nanodendrites were enwrapped with RGO sheets in the composite, as shown in insert in Fig. 1D.

The UV-vis absorption spectra of the products are shown in Fig.2A. From curve (a), it is observed that there is a feature absorption peak of the RGO at about 300 nm.[34-36] As shown on curve (b), typical absorption peak of the AgNDs is located at about 400 nm.[24,37] For the RGO/AgNDs composite, as shown on curve (c), the absorption peaks of two ingredients are present. However, the absorption of the AgNDs was remarkably enhanced due to the presence of the RGO.

Fig.2 (A) UV-vis absorption spectra of the products; (B) Nyquist plots of EIS for products (at the frequency range of 0.1 Hz-100K Hz and the amplitude of 5 mV). Letters in figures: (a) RGO; (b) AgNDs; (c) RGO/AgNDs; (d) bare ITO.

The EIS analysis is known as an effective method to evaluate the interfacial electrochemical property of materials.[38] Our Nyquist plots of the EIS analysis are shown in Fig.2B. Based on the semicircle-like part at high frequency region, the electron transfer resistance (Ret) values are calculated to be 34, 40, 203 and 67 Ω for bare ITO, RGO, AgNDs and RGO/AgNDs composite, respectively. However, the Warburg resistance (Zw) values that resulted from the ionic diffusion/transport in the electrolyte are no significant difference for all kinds of products, since their Nyquist plot slopes at straight line part in low frequency region are similar. From the results of EIS analysis, it can be concluded that the introduction of the RGO decreased the electron transfer resistance of the AgNDs.

3.2 Photoelectric conversion

The measurement results for the photoelectric conversion of the products are shown in Fig. 3. From Fig. 3A, it is observed that the photocurrent produced by RGO is very small, since the conductivity of reduced graphene sheets made the photoelectrons easy to combine with holes.[39] Clearly, the photocurrent of AgNDs was enhanced by RGO,

which will be discussed in follow section. As shown in Fig. 3B, if the electrolyte Na_2S was replaced by KI, the photocurrents produced by AgNDs and RGO/AgNDs composite were all decreased. The phenomenon is explained that the I^-/I_3^- redox couple is corrosive to most metals and quantum dot materials, which resulted in rapid decrease of the photocurrent.[40]

Fig.3. Photoelectric conversion curves of the products: (A) in 0.1 mol/L Na_2S electrolyte solution; (B) in 0.1 mol/L KI electrolyte solution; (C) effect of GO amount (as inset) added in electrodeposition solution; (D) effect of electrodeposition time (as inset).

The effect factors on the photocurrent were further studied by a series of experiments, and the results are shown in Fig.3C and 3D. According to the results in literature,[41] the amount of GO affected the structure and property of the composite as-formed. In typical preparation, 400 μg GO was added in electrodeposition solution. If the amount of GO added in electrodeposition solution was increased or decreased, the photocurrents produced by the RGO/AgNDs composite as-prepared were all decreased, as shown in Fig. 3C. The test results show that when the amount of GO added in electrodeposition solution was increased, the AgNDs sparsely and unevenly distributed on aggregated RGO in product, which resulted in the decrease of photocurrent. If the amount of GO was decreased, also, the photocurrent declined since little AgNDs were enwrapped with RGO sheets in product. In addition, the electrodeposition time was typically set at 200 s in composite preparation. When the electrodeposition time was increased or decreased, also, the photocurrents of the RGO/AgNDs composite as-prepared were decreased, as shown in Fig. 3D.

Fig. 4A shows the reproducibility and stability of the photocurrent produced by RGO/AgNDs composite. From the photoelectric conversion curve, it is seen that

RGO/AgNDs composite has a reproducible response to irradiation, and the photocurrent intensity produced under repeat irradiation is unchanged almost. As well known, the voltage at zero current (namely, open-circuit voltage) means the maximum attainable voltage and the flat band potential as well. Fig. 4B shows the change of photocurrents corresponding to change of bias potentials applied to the work electrodes. From the curves, it is observed that the open-circuit voltages are -0.01 V, -0.21 V and -0.29 V for RGO, AgNDs and RGO/AgNDs composite, respectively. Clearly, a largest open-circuit voltage was obtained with RGO/AgNDs composite.

Fig.4. (A) Photoelectric conversion curve of RGO/AgNDs composite under repeated irradiation; (B) Photocurrents versus voltage for different products.

The excellent photoelectrical conversion of RGO/AgNDs composite is explained as follows. First, as reported in literature,[42] the AgNDs can absorb visible-light by so-called surface plasmon resonance (SPR) effect, which facilitated the excitation of the surface electron and interfacial electron transition. Also, the AgNDs exhibit considerable UV light absorption caused by the interband transition (the transition of 4d electrons to the 5sp band), which resulted in much larger proportion of surface electron transition than SPR absorption.[43-45] Therefore, the AgNDs produced a goodish photocurrent under Xe lamp irradiation based on SPR visible light absorption and interband transition UV light absorption. However, there existed the invalid recombination of the photoexcited electron-hole pairs when photoexciting AgNDs themselves. As well-known, the RGO has excellent electrical conductivity and can serve as the acceptor and transporter of the photoexcited electrons. Therefore, the introduction of the RGO decreased the invalid recombination of the photoexcited electron-hole pairs of the AgNDs and promoted charge transfer in RGO/AgNDs

composite. In addition, the Schottky barrier formed in the RGO/AgNDs interface could hinder the recombination of photo-exited electrons with holes. Finally, the presence of RGO enhanced photon absorption and protected the AgNDs from oxidation due to the impermeable nature of RGO. As a result, the RGO/AgNDs composite showed an excellent photoelectrical conversion by the function of RGO on AgNDs.

3.3 Electrochemical sensor for H_2O_2

In advance, the cyclic voltammograms (CVs) of the electrode modified with RGO/AgNDs composite were measured in absence and presence of H_2O_2 respectively, and the results are shown in Fig.5A. On curve (a), the peaks at +0.42 V and −0.38 V are attributed to the oxidation and reduction of AgNDs, respectively.[46-47] Clearly, the presence of H_2O_2 enhanced the reduction peak, as shown on curve (b), which resulted from the catalysis of AgNDs to H_2O_2 reduction. Referring literature,[48] the reduction reactions of H_2O_2 are listed as follows.

$$2\text{RGO-Ag(0)} + H_2O_2 \rightarrow 2\text{RGO-Ag(I)-OH} \quad (1)$$

$$2\text{RGO-Ag(I)-OH} + 2H^+ + 2e^- \rightarrow 2\text{RGO-Ag(0)} + 2H_2O \quad (2)$$

Fig.5. (A) Cyclic voltammograms of the electrode modified with RGO/AgNDs composite in 1 M H_2SO_4 solution (a) and 1 M H_2SO_4 containing 0.3 mM H_2O_2 (b); (B) Current-time curve of the modified electrode towards successive addition of H_2O_2 in 1 M H_2SO_4 solution (insert: the linear relationship between current and H_2O_2 concentration).

Based on the CVs of the modified electrode, the electrochemical response to H_2O_2 was determined at an applied potential -0.3 V.[32] From the current-time curve, as shown in Fig. 5B, it is observed that the RGO/AgNDs composite responded to H_2O_2

sensitively and rapidly, which is explained as follows. On the one hand, the Ag nanodendrites with electrocatalytic activity have large specific surface area, which made the sufficient contact of the electrode surface with H_2O_2 molecules. On the other hand, the presence of the RGO with excellent electrical conductivity promoted the electron transfer of electrode surface. From the insert in Fig.5B, it is obtained that for electrode modified with RGO/AgNDs, the current response was proportional to the H_2O_2 concentration in a linear range from 0.08 mM to 2.65 mM. It has been reported that the electrode modified with nitrogen-doped graphene-silver nanodendrites responded to H_2O_2 concentration in a linear range from 0.1 mM to 80 mM.[27] For the TiO_2 nanotube/RGO/Ag nanoparticles composite, response linear range to H_2O_2 is from 15.5 mM to 50 mM.[49] Clearly, the superiority of our RGO/AgNDs composite is response to H_2O_2, sensitively.

4. Conclusions

In summary, this work prepared a novel RGO/AgNDs composite by one-step electrodeposition. The preparation is fast and environment friendly since no reduction agent and surfactant is involved. The crystallization and morphology of the composites as-prepared were characterized by XRD and SEM respectively, and the production mechanism of the photocurrent and its effect factors were discussed. Based on the photosensitivity of AgNDs and the electroconductivity of RGO, the RGO/AgNDs composite performed excellent photoelectrical conversion, which exhibits the potential for the electrode material of solar cell. In addition, in view of the electrocatalytic activity of AgNDs to H_2O_2, the electrode modified with RGO/AgNDs composite was used to detect H_2O_2, and the results show that the linear range for H_2O_2 detection is from 0.08 mM to 2.65 mM.

Acknowledgments

Support for this work from the National Natural Science Foundation of China (Nos.21275006, 21471001, 20905001, 21071002, 21175001, 51432001) is gratefully acknowledged.

References

1. O'regan B, Grfitzeli M. A low-cost, high-efficiency solar cell based on dye-sensitized colloidal TiO2 films. *Nature*, 1991, **353**, 737-740
2. Asim N, Sopian K, Ahmadi S, Saeedfar K, Alghoul MA, Saadatian O, Zaidi SH. A review on the role of materials science in solar cells. *Renewable and Sustainable Energy Reviews*. 2012, **16**, 5834-5847.
3. Wright M, Uddin A. Organic-inorganic hybrid solar cells: A comparative review. *Sol Energy Mater Sol Cells,* 2012, **107**, 87-111
4. Kouhnavard M, Ikeda S, Ludin N A, Ahmad Khairudin N B, Ghaffari B V, Mat-Teridi M A Ibrahimb M A, Sepeaib S, Sopian, K. A review of semiconductor materials as sensitizers for quantum dot-sensitized solar cells. *Renewable and Sustainable Energy Reviews*, 2014, **37,** 397-407.
5. Geim AK, Novoselov KS. The rise of graphene. *Nat. Mater.* 2007, **6**, 183-191.
6. Liu S, Ou JF, Wang JQ, Liu XH, Yang SR. A simple two-step electrochemical synthesis of graphene sheets film on the ITO electrode as supercapacitors. *J. Appl. Electrochem.*, 2011, **41**, 881-884.
7. Basu S, Bhattacharyya P. Recent developments on graphene and graphene oxide based solid state gas sensors. *Sens Actuators B: Chemical*, 2012, **173,** 1-21.
8. Liu WW, Chai SP, Mohamed AR, Hashim U. Synthesis and characterization of graphene and carbon nanotubes: A review on the past and recent developments. *J. Ind. Eng. Chem*., 2014, **20**, 1171-1185.
9. Yang N, Zhai J, Wang D, Chen Y, Jiang L. Two-dimensional graphene bridges enhanced photoinduced charge transport in dye-sensitized solar cells. *ACS Nano*, 2010, **4**, 887-894.

10. Iwan A, Chuchmała A. Perspectives of applied graphene: Polymer solar cells. *Prog. Polym. Sci.*, 2012, **37**, 1805-1828.

11. Fang X, Li M, Guo K, Liu X, Zhu Y, Sebo B, Zhao X. Graphene-compositing optimization of the properties of dye-sensitized solar cells. *Sol Energy*, 2014, **101**, 176-181.

12. Chen L, He H, Yu H, Cao Y, Yang D. Fabrication and photovoltaic conversion enhancement of graphene/n-Si Schottky barrier solar cells by electrophoretic deposition. *Electrochim Acta,* 2014, **130**, 279-285.

13. Wang S, Wang Y, Zhou LH, Li, JX , Wang SL, Liu HL. Fabrication of an effective electrochemical platform based on graphene and AuNPs for high sensitive detection of trace Cu^{2+}. *Electrochim Acta*, 2014, **132**, 7-14.

14. Chakrabarti MH, Low CT J, Brandon NP, Yufit V, Hashim MA, Irfan MF, Akhtare J, Ruiz-Trejob E, Hussain MA. Progress in the electrochemical modification of graphene-based materials and their applications. *Electrochim Acta*, 2013, **107**, 425-440.

15. Chowdhury S, Balasubramanian R. Graphene/semiconductor nanocomposites (GSNs) for heterogeneous photocatalytic decolorization of wastewaters contaminated with synthetic dyes: A review. *Appl Catal B: Environmental,* 2014, **160-161**, 307-324.

16. Chook SW, Chia CH, Zakaria S, Ayob MK, Chee KL, Huang NM, Neoh HM, Lim HN, Jamal R, Rahman RMFRA. Antibacterial performance of Ag nanoparticles and AgGO nanocomposites prepared via rapid microwave-assisted synthesis method. *Nanoscale Res. Let.,* 2012, **7**, 1-7.

17. Zhang Y, Yuan X, Wang Y, Chen Y. One-pot photochemical synthesis of grapheme composites uniformly deposited with silver nanoparticles and their high catalytic activity towards the reduction of 2-nitroaniline. *J. Mater. Chem.,* 2012, **22**, 7245-7251.

18. Zhang Y, Liu S, Wang L, Qin X, Tian J, Lu W, Chang G, Sun X. One-pot green synthesis of Ag nanoparticles-graphene nanocomposites and their applications in SERS, H_2O_2, and glucose sensing. *RSC Adv*., 2012, **2**, 538-545.

19. Moradi Golsheikh A, Huang NM, Lim HN, Zakaria R, Yin CY. One-step electrodeposition synthesis of silver-nanoparticle-decorated graphene on indium-tin-oxide for enzymeless hydrogen peroxide detection. *Carbon,* 2013, **62**, 405-412.

20. Zhou L, Gu H, Wang C, Zhang J, Lv M, He R. Study on the synthesis and surface enhanced Raman spectroscopy of graphene-based nanocomposites decorated with noble metal nanoparticles. *Colloid Surface A,* 2013, **430**, 103-109.

21. Zhao B, Liu Z, Fu W, Yang H. Construction of 3D electrochemically reduced grapheme oxide–silver nanocomposite film and application as nonenzymatic hydrogen peroxide sensor. Electrochem. Commun., 2013, **27**, 1-4.

22. Chu Y, Wang Z, Pan Q. Constructing robust liquid marbles for miniaturized synthesis of graphene/Ag nanocomposite. *ACS Appl. Mater. Interfaces,* 2014, **6**, 8378-8386.

23. Ahmed I, Wang X, Boualili N, Xu H, Farha R, Goldmann M, Ruhlmann L. Photocatalytic synthesis of silver dendrites using electrostatic hybrid films of porphyrin–polyoxometalate. *Appl Catal A: General*, 2012, **447**, 89-99.

24. Wang X, Liu X, Wang X. Self-assembled synthesis of Ag nanodendrites and their applications to SERS. *J. Mol. Struct.*, 2011, **997**, 64-69.

25. Ye W, Shen C, Tian J, Wang C, Bao L, Gao H. Self-assembled synthesis of SERS-active silver dendrites and photoluminescence properties of a thin porous silicon layer. *Electrochem. Commun.* 2008, **10**, 625–629.

26. Yang Z, Tjiu WW, Fan W, Liu T. Electrodepositing Ag nanodendrites on layered double hydroxides modified glassy carbon electrode: Novel hierarchical structure for hydrogen peroxide detection. *Electrochim Acta*, 2013, **90**, 400-407.

27. Tajabadi MT, Basirun WJ, Lorestani F, Zakaria R, Baradaran S, Amin YM, Mahmoudian MR, Rezayi M, Sookhakian M. Nitrogen-doped graphene-silver nanodendrites for the non-enzymatic detection of hydrogen peroxide. *Electrochim Acta,* 2015, **151,** 126-133.

28. Hummers JWS, Offeman RE. Preparation of graphitic oxide. *J. Am. Chem. Soc.,* 1958, **80**, 1339-1339.

29. Guo HL, Wang XF, Qian QY, Wang FB, Xia XH. A green approach to the synthesis of graphene nanosheets. *ACS nano,* 2009, **3**, 2653-2659.

30. Zhang D, Fang Y, Miao Z, Ma M, Chen, Q. Electrochemical determination of dissolved oxygen based on three dimensional electrosynthesis of silver nanodendrites electrode. *J. Appl. Electrochem.* 2014, **44**, 419-425.

31. Liu B, Ding C, Xiao B, Cui L, Wang M. Electrocatalytic dechlorination of chloroacetic acids on silver nanodendrites electrode. *Mater. Sci. Eng. C,* 2014, **37**, 108-112.

32. Qin X, Wang H, Wang X, Miao Z, Fang Y, Chen Q, Shao X. Synthesis of dendritic silver nanostructures and their application in hydrogen peroxide electroreduction. *Electrochim Acta*, 2011, **56**, 3170-3174.

33. Liu B, Wang M. Electrodeposition of dendritic silver nanostructures and their application as hydrogen peroxide sensor. *J. Electrochem. Sci.*, 2013, **8**, 8572-8578.

34. Zhang J, Yang H, Shen G, Cheng P, Zhang J, Guo S. Reduction of graphene oxide via L-ascorbic acid. *Chem. Commun.,* 2010, **46**, 1112–1114.

35. Liu S, Tian J, Wang L, Sun X. A method for the production of reduced graphene oxide using benzylamine as a reducing and stabilizing agent and its subsequent decoration with Ag nanoparticles for enzymeless hydrogen peroxide detection. *Carbon*, 2011, **49**, 3158-3164.

36. Robinson JT, Tabakman SM, Liang Y, Wang H, Sanchez CH, Vinh D, Dai H. Ultrasmall reduced graphene oxide with high near-infrared absorbance for photothermal therapy. *J. Am. Chem. Soc.,* 2011, **133**, 6825-6831.

37. Sun L, Liu A, Tao X, Zhao Y. A green method for synthesis of silver nanodendrites. *J. Mater. Sci.* 2011, **46**, 839-845.

38. Chen X, Wang Y, Zhou J, Yan W, Li X, Zhu JJ. Electrochemical Impedance Immunosensor Based on Three-Dimensionally Ordered Macroporous Gold Film. *Anal. Chem.*, 2008, **80**, 2133–2140.

39. Yan Y, Liu Q, Du X, Qian J, Mao H, Wang K. Visible light photoelectrochemical sensor for ultrasensitive determination of dopamine based on synergistic effect of grapheme quantum dots and TiO_2nanoparticles, *Anal. Chim. Acta*, 2014, **853**, 258-264.

40. Li L, Yang X, Gao J, Tian H, Zhao J, Hagfeldt A, Sun L. Highly efficient CdS quantum dot-sensitized solar cells based on a modified polysulfide electrolyte. *J. Am. Chem. Soc.,* 2011, **133**, 8458-8460.

41. Wang A, Wang H, Zhang S, Mao C, Song J, Niu H, Jin B, Tian Y. Controlled synthesis of nickel sulfide/graphene oxide nanocomposite for high-performance supercapacitor. *Appl. Surf. Sci.,* 2013, **282**, 704-708.

42. Mulpur P, Podila R, Lingam K, Vemula SK, Ramamurthy SS, Kamisetti V, Rao AM. Amplification of Surface Plasmon Coupled Emission from Graphene-Ag Hybrid Films. *J. Phys. Chem. C*, 2013, **117**, 17205-17210.

43. Kamat PV. Photophysical, photochemical and photocatalytic aspects of metal nanoparticles. *J. Phys. Chem. B,* 2002, **106**, 7729-7744.

44. Chen X, Zheng Z, Ke X, Jaatinen E, Xie T, Wang D, Guo C, Zhao J, Zhu H. Supported silver nanoparticles as photocatalysts under ultraviolet and visible light irradiation, *Green Chem.*, 2010, **12**, 414-419.

45. Voisin C, Del FN, Christofilos D, Vallee F. Ultrafast electron dynamics and optical nonlinearities in metal nanoparticles. *J. Phys. Chem. B,* 2001, **105**, 2264-2280.

46. Zhao W, Wang H, Qin X, Wang X, Zhao Z, Miao Z, Chen L, Shan M, Fang Y, Chen Q. A novel nonenzymatic hydrogen peroxide sensor based on multi-wall carbon nanotube/silver nanoparticle nanohybrids modified gold electrode. *Talanta*, 2009, **80**, 1029-1033.

47. Afraz A, Rafati A A, Hajian A. Analytical sensing of hydrogen peroxide on Ag nanoparticles-multiwalled carbon nanotube-modified glassy carbon electrode. *J. Solid State Electrochem.,* 2013, **17**, 2017-2025.

48. Maggs FT, Sutton D. Some Aspects of the Catalytic Decomposition of Concentrated Hydrogen Peroxide by Silver. Part1. -The Solubility and Rate of Solution of Silver. *Trans Faraday Soc.* 1958, **54**, 1861-1870.

49. Wang W, Xie Y, Xia C, Du H, Tian F. Titanium dioxide nanotube arrays modified with a nanocomposite of silver nanoparticles and reduced graphene oxide for electrochemical sensing. Microchim Acta, 2014, **181**, 1325-1331.

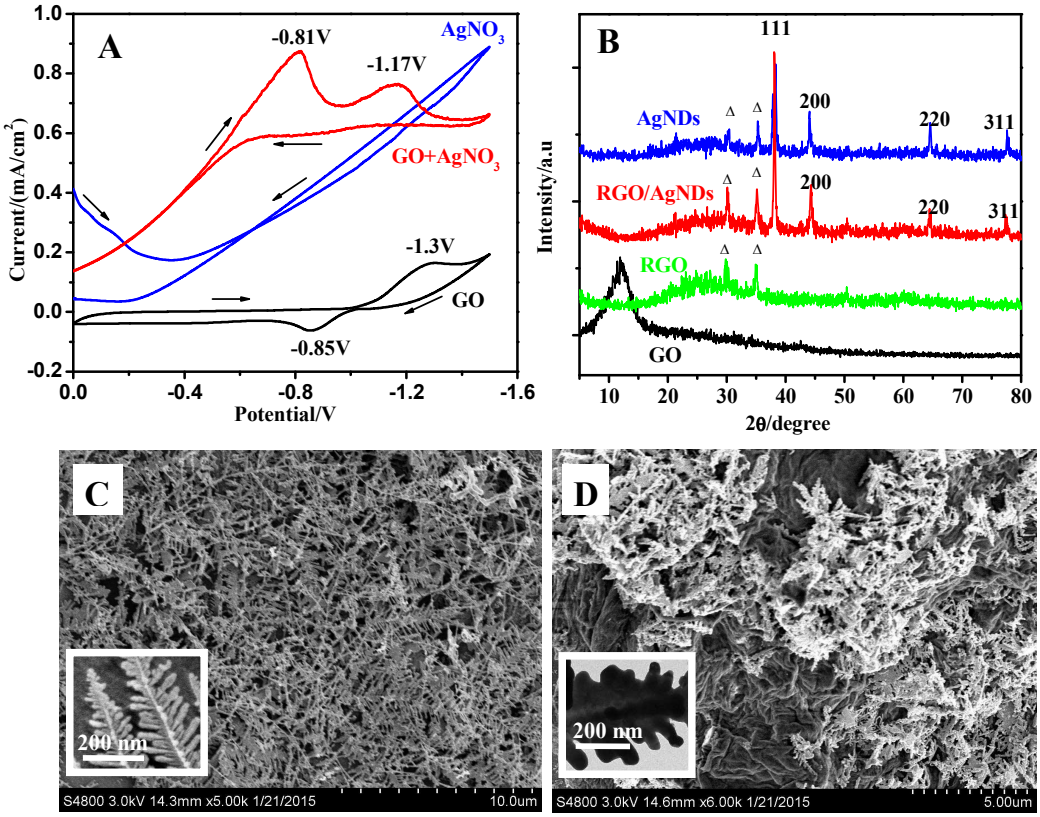

Fig.1 (A) The cycle voltammograms obtained in different solutions (at scan rate of 25 mVs^{-1}); (B) XRD patterns of the products; (C) SEM image of pure Ag product (insert: enlarged part image); (D) SEM image of RGO/AgNDs composite (insert: enlarged part image of TEM).

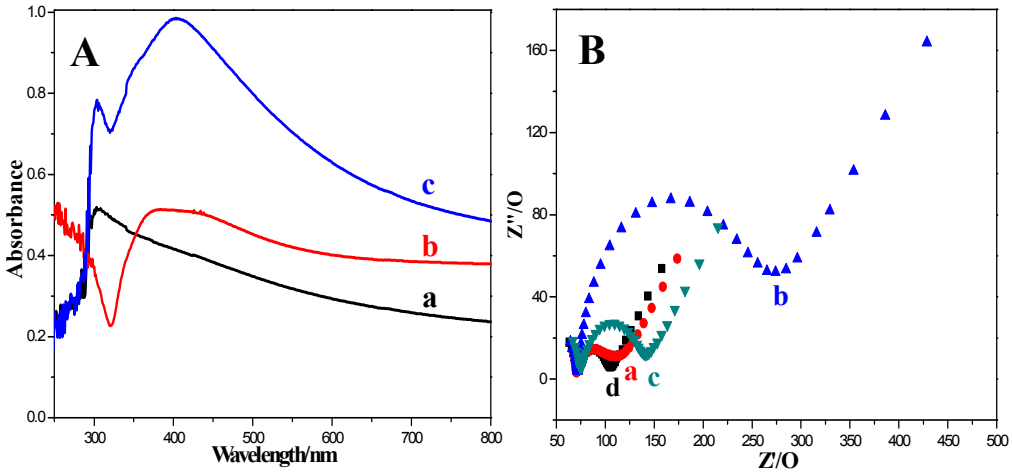

Fig.2 (A) UV-vis absorption spectra of the products; (B) Nyquist plots of EIS for products (at the frequency range of 0.1 Hz-100K Hz and the amplitude of 5 mV). Letters in figures: (a) RGO; (b) AgNDs; (c) RGO/AgNDs; (d) bare ITO.

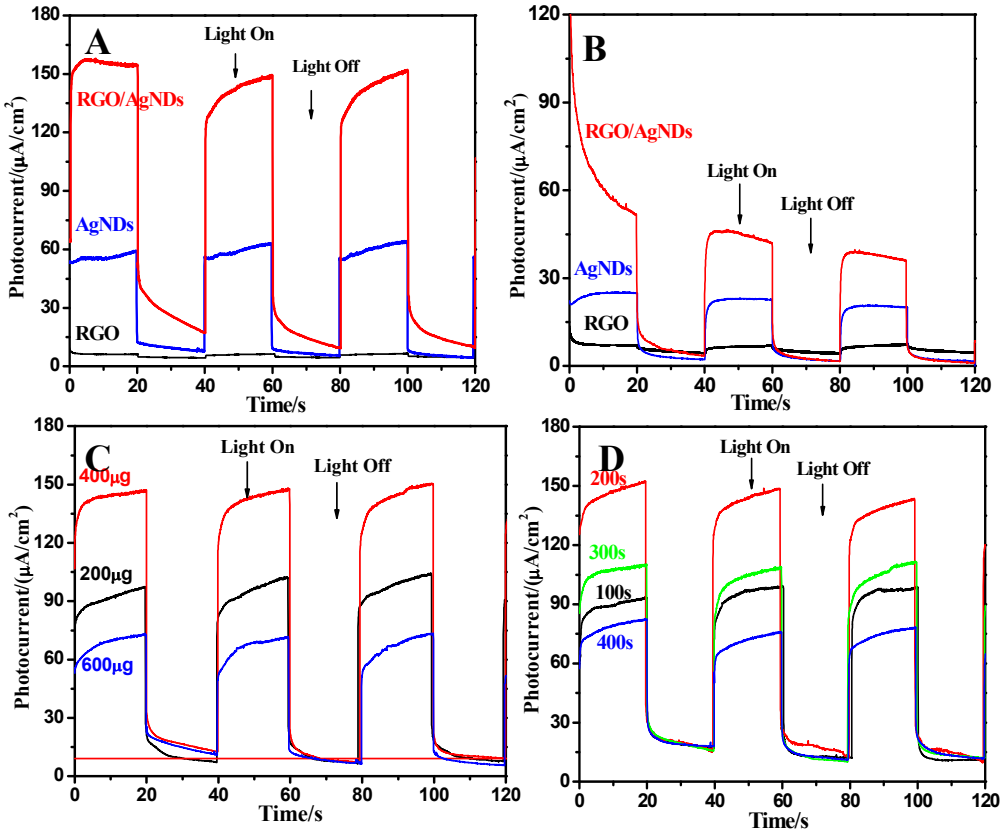

Fig.3. Photoelectric conversion curves of the products: (A) in 0.1 mol/L Na_2S electrolyte solution; (B) in 0.1 mol/L KI electrolyte solution; (C) effect of GO amount (as inset) added in electrodeposition solution; (D) effect of electrodeposition time (as inset).

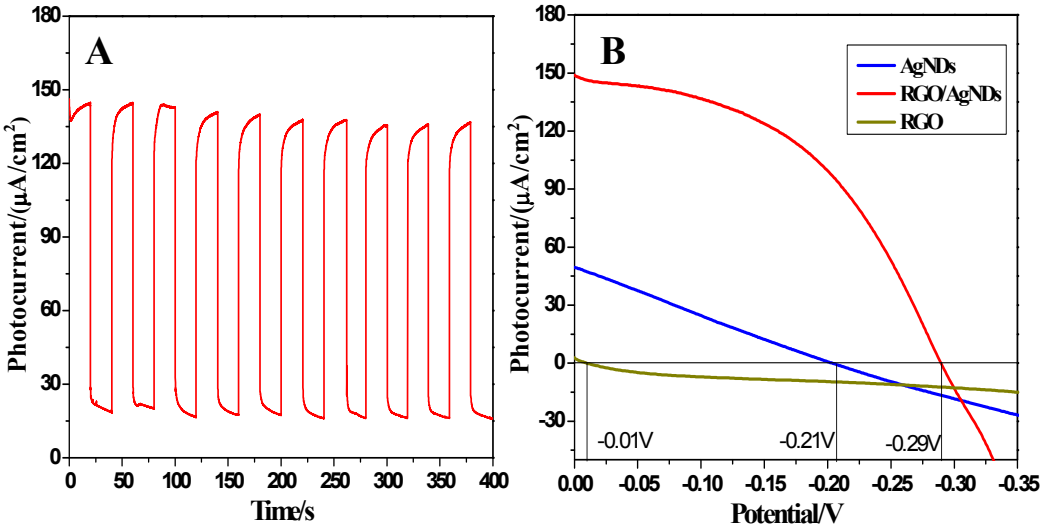

Fig.4. (A) Photoelectric conversion curve of RGO/AgNDs composite under repeated irradiation; (B) Photocurrents versus voltage for different products.

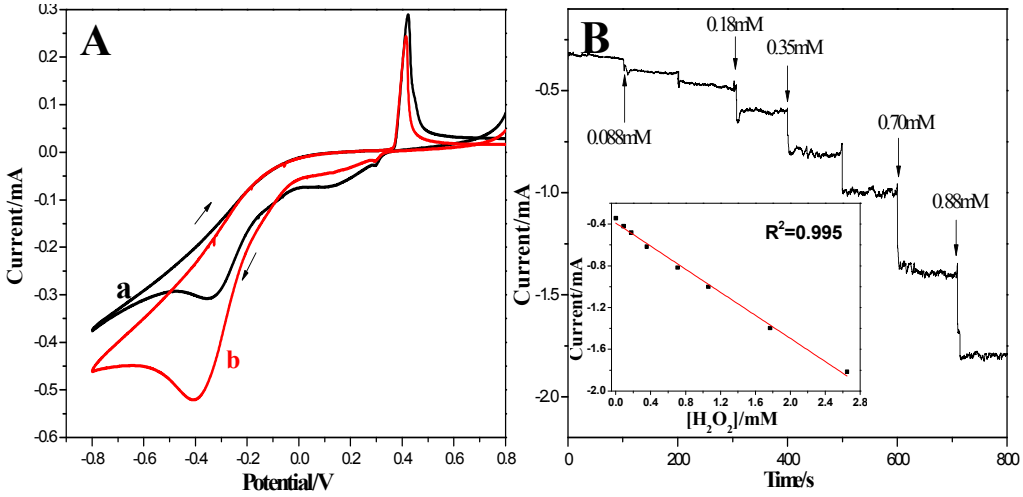

Fig.5. (A) Cyclic voltammograms of the electrode modified with RGO/AgNDs composite in 1 M H_2SO_4 solution (a) and 1 M H_2SO_4 containing 0.3 mM H_2O_2 (b); (B) Current-time curve of the modified electrode towards successive addition of H_2O_2 in 1 M H_2SO_4 solution (insert: the linear relationship between current and H_2O_2 concentration).